Multiscale structure of cellulose microfibrils in regenerated cellulose fibers

Jiliang Liu, Herbert Sixta, Yu Ogawa, Michael Hummel, Michael Sztucki, Yoshiharu Nishiyama, Manfred Burghammer

To cite this version:

Jiliang Liu, Herbert Sixta, Yu Ogawa, Michael Hummel, Michael Sztucki, et al.. Multiscale structure of cellulose microfibrils in regenerated cellulose fibers. Carbohydrate Polymers, 2024, 324, pp.121512. 10.1016/j.carbpol.2023.121512 . hal-04876845

HAL Id: hal-04876845
https://hal.science/hal-04876845v1

Submitted on 9 Jan 2025

Multiscale structure of cellulose microfibrils in regenerated cellulose fibers

Jiliang Liu[1], Hebert Sixta[2], Yu Ogawa[3], Michael Hummel[2], Michael Sztucki[1], Yoshiharu Nishiyama[3], Manfred Burghammer[1]*.*

1. European Synchrotron Radiation Facility, ESRF, 38000 Grenoble, France

2. Department of Bioproducts and Biosystem, Aalto University, Finland

3. University Grenoble Alpes, CNRS, CERMAV, 38000 Grenoble, France

KEYWORDS: Microfibrils(MF), cellulose elementary fibrils(CEFs), scanning X-ray micro/nano diffraction(SXM/N), spinning process, porosity.

ABSTRACT

Cellulose in solution can be assembled into textile fibers by wet-spinning (Viscose etc.) or dry-jet wet-spinning (Lyocell, Ioncell etc.), which lead to significant differences in the mechanical properties of fibers. We use scanning X-ray microdiffraction (SXM) to reveal in unprecedented detail the arrangement of cellulose fibrils in the “skin-core” morphology of the fibers. The cellulose elementary fibrils have a ribbon-like cross sectional shape of about 6 x 2 nm, which are packed into microfibrils (MFs) ~ 100 nm in diameter. Our SXM studies demonstrate that MFs within Ioncell fibers are composed of elementary fibrils with homogeneous morphologies. Furthermore, the stacking of cellulose molecular sheets within elementary fibrils of Viscose fibers is preferentially along the 010 direction, while those of Ioncell fibers preferably stack in the 1-10 direction. The better structural regularities of elementary fibrils give Ioncell fibers mechanical properties and a wet strength far superior to those of Viscose fibers.

1. INTRODUCTION

Regenerated cellulose fibers (RCFs) are important textile fibers due to their sustainable nature and high wearing comfort. Although they currently account for only 6-7% of the global textile market, their use is rapidly increasing (Azimi B. et al., 2022; Hermanutz, F. et al., 2019). Viscose fibers, the most common RCFs, are produced by a wet-spinning process, a mature but environmentally harmful technique due to the use of toxic carbon disulfide (CS2) (Azimi B. et al., 2022). The second category of regenerated fibers is generally represented by the Lyocell process, in this work by a specific Lyocell process version called Ioncell process, where cellulose dissolved in a direct solvent is spun in a dry jet wet spinning process, which is environmentally friendly and produces fibers with high strength (Azimi B. et al., 2022; Hermanutz, F. et al., 2019, Elsayed S. et al. 2012, Nishiyama Y. et al 2019). The Ioncell solvent, 1,5-diazabicyclo[4.3.0]non-5-enium acetate utilized in this process, was identified as an excellent cellulose solvent for dry-jet wet fiber spinning (Asaadi, S. et al 2018). Fibers spun by the Ioncell process exhibit excellent mechanical properties, especially high tenacity which is less affected by hydration (Asaadi, S. et al 2018). The variations of mechanical properties of the fibers with different spinning processes suggest that cellulose forms distinct structures for different spinning processes (Abu-Rous, M. et al 2006). Using SEM and X-ray microdiffraction, the “skin-core” morphology of Ioncell cellulose fibers has been characterized on the micron scale (Müller, M. et al 2000; Moss, C. E. et al., 2002). Within the “core” region, cellulose fibrils consist of microfibrils (MFs) with a diameter in the 100 nm range (Schuster, K. C., et al 2003). It was assumed that the MFs are composed of crystallized cellulose elementary fibrils and that the greater crystallinity index (CI) of elementary fibrils of STandard Ioncell fibers (IONCELL-ST) and High-Tenacity Ioncell fibers (IONCELL-HT) compared to regular cellulose viscose fibers (to be called regular fibers or abbreviated as CV in the following) could impact the mechanical properties of the regenerated fibers. Nevertheless, conclusive evidence for this was lacking. The mesostructure of elementary fibrils in the ~10's nm is beyond the resolution limit of SEM. Transmission electron microscopy (TEM) has the necessary resolution to visualize regenerated cellulose crystals but is unable to detect the elementary fibrils within the microfibrils due to the limited penetration depth of electrons (Abu-Rous et al., 2006; Ogawa Y. et al 2019). X–ray diffraction is an alternative technique for investigating the structure of materials that is capable of penetrating significant sample thickness and generating structural information with molecular-scale resolution (Liu J. et al 2022). In this work, we apply scanning X-ray Micro/Nanodiffraction (SXM/N) to IONCELL-HT, IONCELL-ST and CV to characterize their structure over a wide length scale, thereby offering insight into the molecular basis of their distinct mechanical properties. These studies reveal the "skin–core" morphology of different regenerated fibers at the micrometer scale and the morphology and polymorphs of elementary fibrils of IONCELL-HT, IONCELL-ST and CV. This multiscale structural information provides insights into the way how the structures of fibers at different length scale influences their mechanical properties.

2. MATERIALS AND METHODS

2.1 Fiber generating process.

High tenacity Ioncell fibers (IONCELL-HT) were spun from a solution of a Buckeye V5 pulp in [DBNH][OAc], Ioncell standard fibers (IONCELL-ST) were produced from a commercial birch pre-hydrolysis kraft pulp (PHK) as described earlier (Moriam K. et al 2021). The Viscose fiber (CV) is a commercial unmodified viscose staple fiber marketed as normal or standard viscose fiber. These fibers are white textile fibers, as shown in Figure S17. The process details have been presented in the Supplementary Materials. The mechanical properties of RCFs are shown in Table S3.

2.2 Scanning X–ray Micro/Nano diffraction.

Scanning X-ray microdiffraction experiments were carried out at the Microfocus Beamline ID13 at the European Synchrotron Radiation Facility (ESRF) with an X–ray energy of 13 keV (wavelength 0.953 Å). Beryllium Compound refractive lenses (CRL) focused the monochromatic beam down to a size of 2.5 μm at the sample position. An ion chamber and a circular guard aperture of 30 μm in diameter were put upstream the sample to reduce the diffuse background scattering. The total flux was ~10^{12} photons/s. Downstream the sample, a beam stop, blocking the direct beam, and a 2D photon counting pixel array detector (Eiger X 4M detector, DECTRIS Ltd., 2167×2070 pixels of 75 μm in size) were positioned. For scanning X–ray nano diffraction experiment, a Silicon Nano Focusing Lens (NFL) at Nanofocus hutch focuses the beam to 250 nm with a total flux of ~10^{11} Photons/s. The downstream setup is similar to the microdiffraction experiments.

2.3 SAXS experiment.

High-resolution SAXS (HR SAXS) measurements were carried out at the TrUSAXS beamline ID02 at the European Synchrotron Radiation Facility (ESRF) at an X-ray energy of 12.23 keV (wavelength 1.014 Å) (Narayanan, M., et al 2022). The beam size was about 100 μm in diameter, the sample to detector distance was set to 2 m. 2D SAXS spectra were recorded using an Eiger2X 4M pixel detector (DECTRIS, 2167×2070 pixels of size 75 μm), corrected, normalized and azimuthally averaged according to standard ID02 procedures. To characterize the shape of the oriented fibers (equatorial profile), a partial azimuthal averaging was performed in an angular range ±5° around the direction perpendicular to the fiber axes.

2.4 Spectroscopy and Microscopy image.

FT-IR measurements were conducted using a Spectrum Two spectrometer (Perkin Elmer) operated under attenuated total reflection (ATR) mode. The specimen was immersed in heavy water and positioned in the spectrometer with the fiber axis either parallel (p) or perpendicular (v) to the incident IR beam direction. Spectra were acquired at ambient temperature condition and averaged over 16 scans with a resolution of 4 cm^{-1}.

All solid-state NMR measurements were conducted using a Bruker Avance III 400 MHz spectrometer operating at 100.6 MHz for 13C. The specimens were packed into a zirconia specimen rotor. The magic angle spinning rate was 12 kHz. 13C cross-polarization (CP/MAS) NMR spectra were measured with a cross-polarization contact time of 2 ms and a delay time of 2 s. Peak fitting analysis was done using the Gnuplot software (Williams, T. and Kelley, C. 2011).

2.5 Data analysis of SAXS/WAXS

The Crystallinity Index (CI) and Degree of Preferred Orientation (DPO) of cellulose fibrils have been determined by fitting WAXS patterns of SXM. Figure S2a-b shows the fitting of equatorial intensity profile with three Voigt functions correlated to featured reflection (1 0 0), (1 1 0) and (0 2 0) and a diffuse amorphous background. The CI is determined by:

$$CI = \frac{I_{100} + I_{110} + I_{020}}{I_{100} + I_{110} + I_{020} + I_{amorphous}}$$

The azimuthal distribution of feature reflection (0 2 0) with Voigt functions (Figure S2c-d). The full width maximum (FWHM) of the fitted Voigt function determine the DPO.

The Voigt function $V(x, \mu, \sigma, \gamma)$ is written as:[1]

$$V(x, \mu, \sigma, \gamma) = \int_{-\infty}^{\infty} G(x', \mu, \sigma) L(x - x', \mu, \gamma) dx'$$

$$G(x, \mu, \sigma) = \frac{e^{-(x-\mu)^2/(2\sigma^2)}}{\sigma\sqrt{2\pi}}$$

$$L(x, \mu, \gamma) = \frac{\gamma}{\pi((x-\mu)^2 + \gamma^2)}$$

Where $G(x, \mu, \sigma)$ is a Gaussian function and $L(x, \mu, \gamma)$ is a Lorentz function, both are centered at μ.

The FWHM of the Voigt function is determined as follow:[1]

$$f_V \approx 0.5346 F_L + \sqrt{0.2166 f_L^2 + f_G^2}$$

Where f_G is FWHM of the Gaussian function:

$$f_G = 2\sigma\sqrt{2 \in (2)}$$

And f_L is FWHM of the Lorentz function:

$$f_L = 2\gamma$$

3. RESULTS

3.1 Skin–Core morphology and its correlated structural features.

SXM/N reveals that IONCELL-ST, IONCELL-HT and regular fibers all show a “skin–core” morphology. The “skin” consists of highly crystallized cellulose fibrils and nano voids (Abu-Rous, M. et al 2006). The strong contrast of electron density between cellulose crystallites and elongated air voids gives rise to the strong anisotropic surface scattering signal at small angles, $q < 0.05$ Å^{-1}. Figure 1 a-c and Figure S1 d-f show the “skin” characterized by Small Angle X-ray Scattering (SAXS) patterns for all three types of fibers. The thickness of the “skin” for IONCELL-ST and IONCELL-HT is not uniform and can vary between 250 and 500 nm, while CV showed a thicker skin of about 750 nm. The Crystallinity Index (CI) and Degree of Preferred Orientation (DPO) of cellulose fibrils have been determined by fitting Wide Angle X-ray Scattering (WAXS) patterns of SXM. As shown in Figure 1a-c and Figure S3, IONCELL-ST and HT exhibit higher parameter values for crystallinity index and degree of orientation than CV. Furthermore, the “skin-core” morphology also manifests in the maps of these parameters for CV (Figure 1 and Figure S3 f and i). However, such contrast is small for the IONCELL-ST and IONCELL-HT. (Figure 1 and Figure S3 d, g, e, h) The variations in degree of orientation are concomitant with the variation in crystallinity index, both decreasing from the “skin” towards the “core” for all fibers.

The solid-state NMR spectra in Figure 1d also confirms that IONCELL-HT has less intense signals from the surface and the amorphous fraction of cellulose microfibrils compared to IONCELL-ST and CV. The crystallinity index (CI) estimates based on the peak fitting of C4 and C6 regions of NMR spectra are in descending order IONCELL-HT > IONCELL-ST > CV

(Figure S4 and Table S1), which is consistent with the SXM/N results. This indicates that the crystallization of the cellulose proceeds more uniformly in dry-jet wet Ioncell spinning. An interesting phenomenon is that according to the polarized ATR FTIR spectra shown in Figure 1e, IONCELL-ST and CV have a relatively high degree of orientation, while IONCELL-HT exhibits higher orientation disorder which is correlated to the conformity between the parallel and perpendicular spectra. This might be due to the high fibrillation tendency of IONCELL-HT under the lateral compression the fibers experienced during the ATR-FTIR measurements.

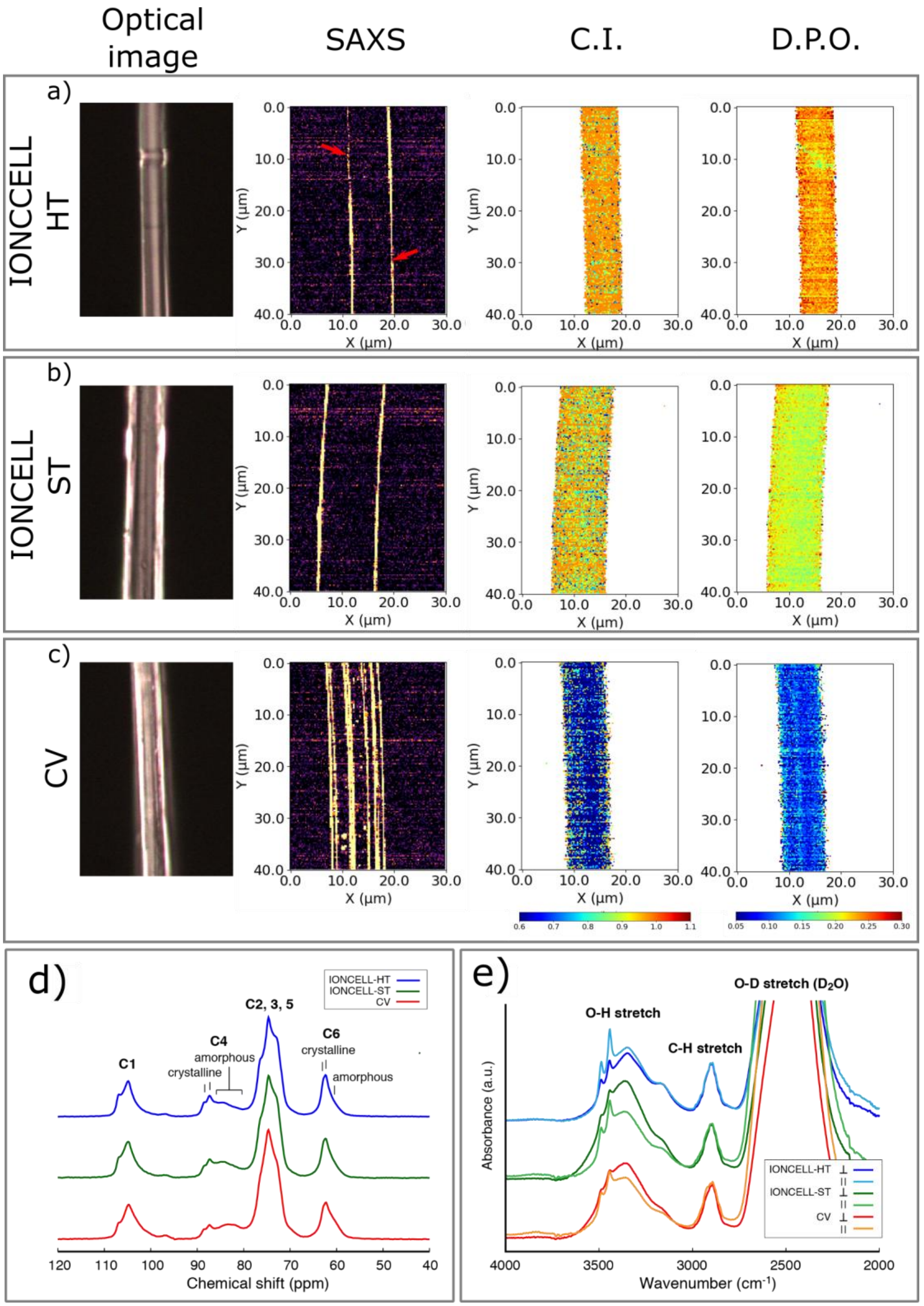

Figure 1. The "skin–core" morphology of IONCELL-HT, IONCELL-ST and CV are revealed by SXN. a)–c) the optical images and the maps of integral intensity of SAXS patterns, CI and

DPO of correlated RCFs. The thickness of “skin” of a) is not uniform. Weak scattering power indicates extreme thin “skin” (arrowheads pointed). d) solid-state 13C NMR and e) ATR-FTIR spectra of IONCELL-HT, IONCELL-ST and CV.

3.2 Meso structure determined by SAXS.

SAXS measurements were performed to characterize the submicron and meso-structure of the fibers. From SEM data, the microfibrils of CV have a lateral size of ~100 nm (submicron) (Schuster, K. C. et al 2003). The high resolution SAXS in Figure S8a demonstrates that all fibers exhibit SAXS signals with a comparable exponent determined by Porod fitting to about -4. This suggests that the microfibrils have a smooth interface within the fibers (Hammouda, B. 2012). The maps of SAXS of Figure 1a-c shows that SAXS patterns varied from skin to core. The equatorial SAXS patterns from the “core” determined by SXM reveal structural variations on the mesoscale among different types of fibers. As shown in Figure 3, the equatorial SAXS curves of IONCELL-HT and IONCELL-ST, but not of CV, contain an interference maximum at $q = 0.17$ $Å^{-1}$. This interference peak is related to the inter-fibrillar structure factor (Lenz, J. et al. 1992). To understand the structures of the constituent elementary fibrils, we conducted Monte Carlo simulations using various models (Figure 2a and Figure S10a). The cylinder model is the most commonly used model to approximate inter–fibril organization. It was used for accurate simulation of the arrangement of elementary fibrils in flax fibers (Müller, M. et al 1998). However, the elementary fibrils within regenerated cellulose types are quite different from those in natural cellulose fibers. While the elementary fibrils of flax fibers have cellulose Iβ structure and low density due to amorphous components such as hemicellulose and lignin, the crystal structure of regenerated fibers is cellulose II with the high cellulose purity leading to higher density. At high density of elementary fibrils the scattering contribution from interference among them is no longer negligible. TEM and AFM studies have shown that the regenerated cellulose II crystals have a rectangular shape with a width of 3-10 nm (Hirota, M. et al 2012; Sèbe, G. et al 2012). Figure S10d shows that the simple cylinder model cannot accurately simulate this interference pattern. Thus, we introduced a rectangular model in the Monte Carlo simulation. A model having an elongated rectangular shape about 6 nm x 2 nm gives the best fitting results as shown in Figure 3a. The equatorial SAXS curve of IONCELL-HT fiber shows the most distinct interference patterns, even including a second order of reflection at a q of ~0.4 $Å^{-1}$, which is well in agreement with the simulated pattern. This indicates that the elementary fibrils of IONCELL-HT have greater homogeneities in both size and orientation of elementary fibrils. The equatorial SAXS curve of IONCELL-ST, as shown in Figure 3b, also exhibits an interference shoulder at 0.17 $Å^{-1}$, but this interference pattern is flattened and does not exhibit an obvious second order reflection. The fitting result suggests size variations of elementary fibrils in IONCELL-ST. No distinct interference peaks are presented in the equatorial SAXS curve of CV, as shown in Figure 3c. Based on these fitting results we can conclude that the elementary fibrils of CV are highly polydisperse in size and exhibit significant randomness of orientation.

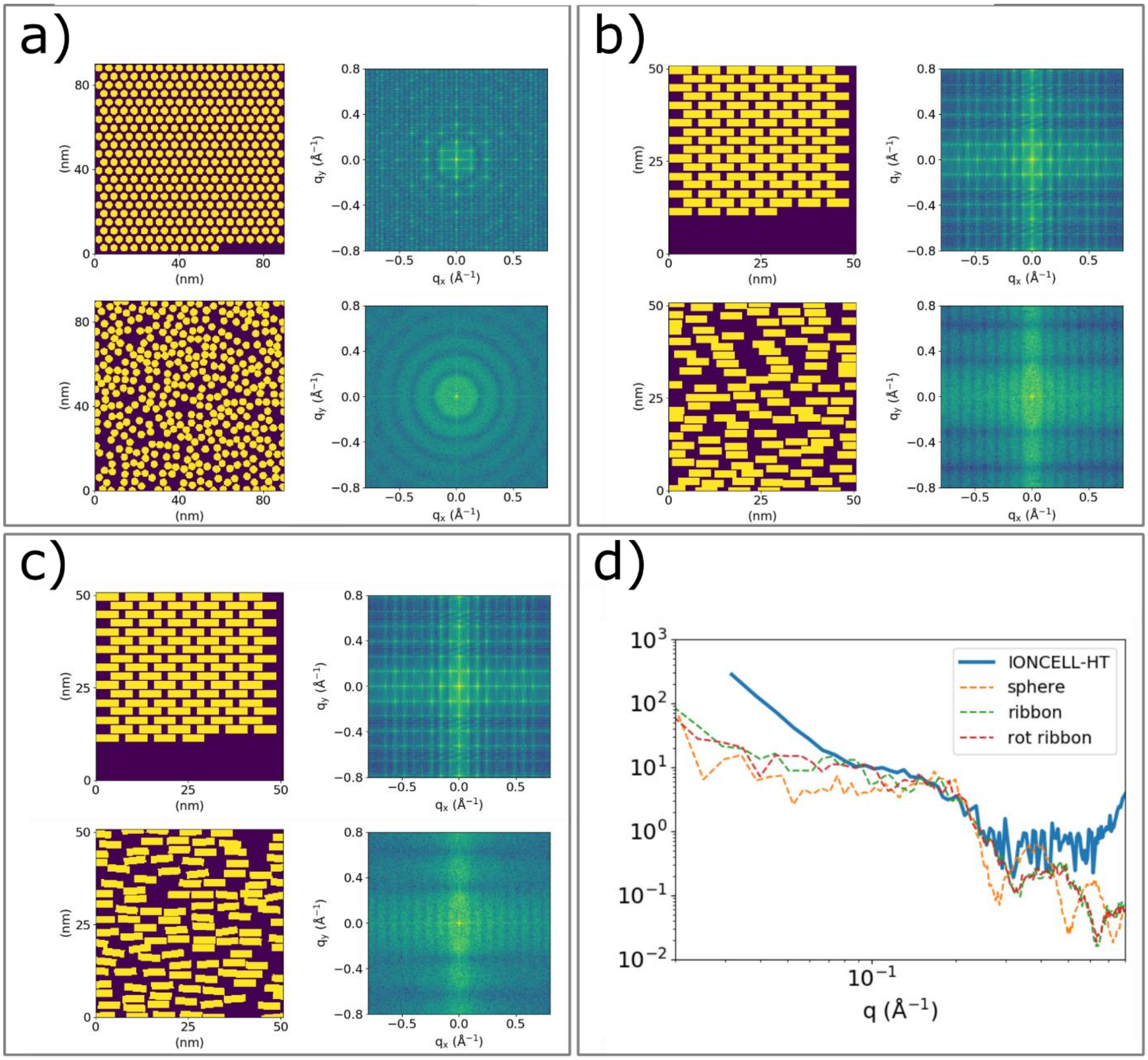

Figure 2. The Monte Carlo simulation of different CEFs models. a) the simulation of circles with radius of 1.4 nm; b) the simulation of ribbon with length of 6 nm and width of 2nm; c) the simulation of ribbon with the length of 6 nm and the width of 2nm and the random deviated orientation to elongated axis.

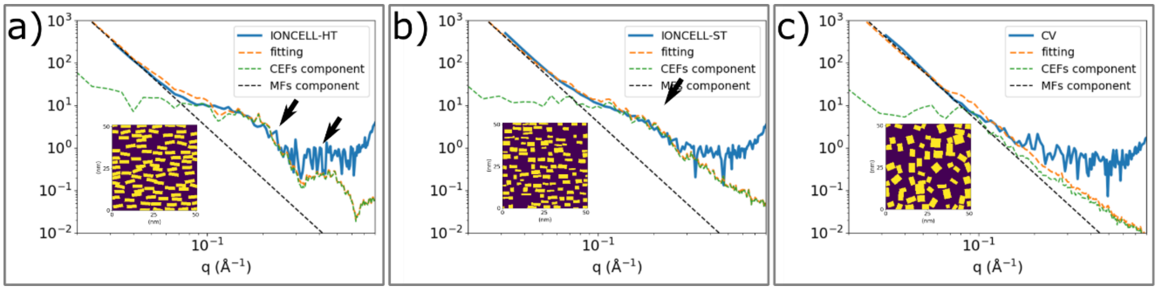

Figure 3. The SXM SAXS curves are fitted by the Monte Carlo simulation using different ribbon models. The inset shows the final state of ribbon–shaped elementary fibrils (CEFs) after 2000 random walking. a) fitting of the equatorial SAXS curve of IONCELL-HT, the volume ratio of CEFs within simulation box is 40%, CEFs are homogeneous. Two featured reflections of the simulated interference pattern, highlighted by arrowhead, could be correlated with the interference patterns in the equatorial SAXS curve of IONCELL-HT; b) fitting of the equatorial SAXS curve of IONCELL-ST, the volume ratio is 30%, the obvious size variations of CEFs are observed; c) fitting of the equatorial SAXS curve of regular fibers (CV), volume ratio is 35%, both size and orientation of CEFs are randomly varied. The porosities due to the interface between MFs contribute to the SAXS curves at q < 0.06 Å-1. The black dash curves in plot a), b) and c) use the power of q obtained from HR SAXS shown in Figure S8a.

3.3 Molecular structure determined by WAXS.

Higher resolution details of the elementary fibril structure can be analyzed from the wide-angle scattering data of SXM. Figures S6 and S7 show that even though the equatorial WAXS profiles of SXM/N exhibit some variations within an individual fiber, different types of fibers appear to have different predominant equatorial WAXS profiles. From Figure 4 and Figure S12b, we find that the equatorial WAXS curves of the “core” of IONCELL-HT and IONCELL-ST have a more intense 110 reflection than 020, whereas CV has stronger 020 reflection than 110. This is a clear evidence of significant differences in the molecular organization of the two fibers. Figure S12c shows that models with elementary fibrils stacking along the 010 direction predict a WAXS profile with a stronger 020 reflection similar to the experimental feature of CV. Figure 4 shows that the intensity profiles calculated from the models having molecule sheets stacking along the 1-10 direction predict the 110 reflection to appear stronger than the 020, similar to that observed for IONCELL-HT and IONCELL-ST also indicating different molecular stacking in these fibers compared to CV.

The variation of the equatorial WAXS profile could be further modeled in terms of the elementary fibrils cross-sectional shapes and the arrangement of cellulose molecules inside. The size of elementary fibrils is estimated by the fitting of the equatorial SAXS curve, which indicates an elongated cross section of the elementary fibrils with dimensions of roughly 6 nm x 2 nm. This means that individual elementary fibrils can typically have 7 unit cells in either a or b directions. The diffraction pattern of a small crystal, of which the number of unit cells is less than about 10 in one direction, will be affected by its crystal shape and the interference scattering between molecules within the crystal (Guinier, A., 199). We fit the equatorial WAXS profiles by nine discrete models.(Figure 5) Table S2 shows that CV mostly contains cellulose sheets stacking along the 010 direction, whereas IONCELL-HT and IONCELL-ST cellulose are stacking along both 010 and 1-10 direction.

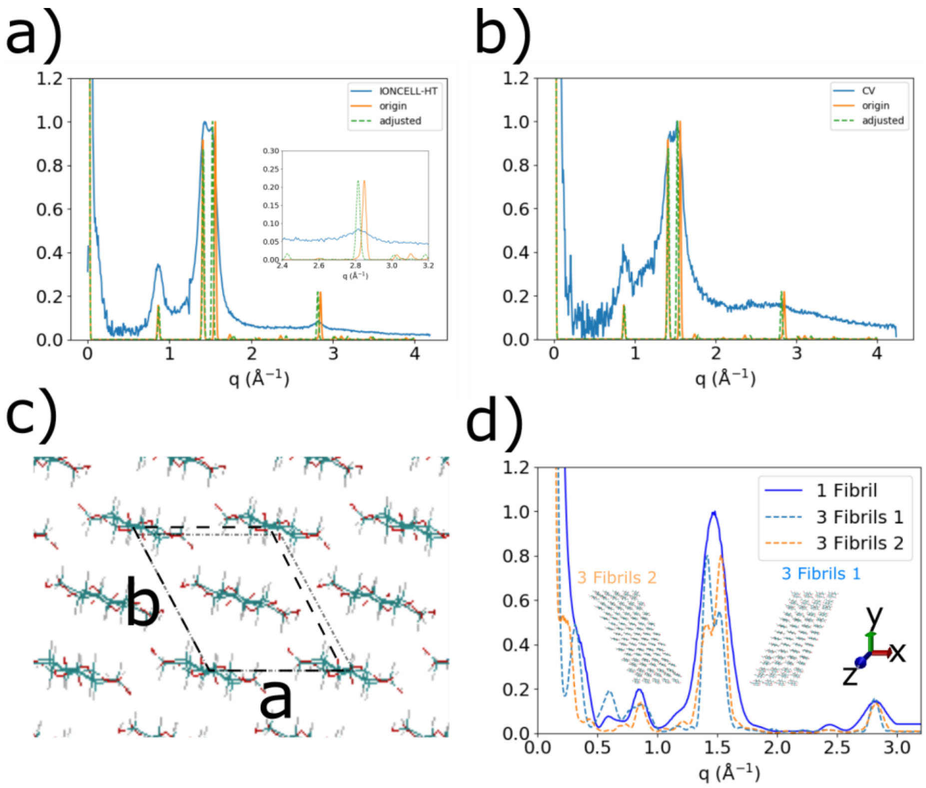

Figure 4. WAXS data shows a structural difference between the theoretical cellulose II crystal and real elementary fibrils. The equatorial intensity profile of a) IONCELL-HT and b) CV is compared with the theoretical and fitted lattice constant. The fitted lattice constant gives the adjusted peak position, which could be well consisted with patterns of equatorial intensity profile of a) IONCELL-HT and b) CV. c) the new unit cell constructed by new lattice constant (black dash line). (grey dot dash line is the unit cell of theoretical lattice constant of cellulose II) d) Different morphologies of elementary fibrils vary the intensity profiles of WAXS. The cellulose stacking along different direction varies intensity ratio of reflection 020 to 110.

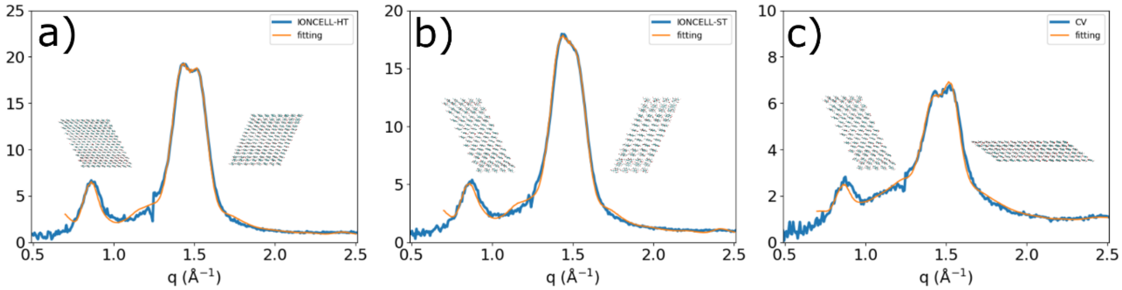

Figure 5. The equatorial WAXS profiles are fitted by the combination of the equatorial intensity profiles of six elementary fibrils (CEFs) models. Fitting results of a) IONCELL-HT and b) IONCELL-ST indicate that the cellulose molecule sheets within CEFs of IONCELL-HT and IONCELL-ST prefer to stack along (1 -1 0) direction; c) fitting result of CV indicates that the cellulose molecule sheets within CEFs of CV stack along (0 1 0) direction.

4. DISCUSSION

4.1 The variations of “skin-core” for different fibers.

All regenerated cellulose fibers we studied are found to have “skin-core” morphologies. The thicknesses of skin for IONCELL-HT and IONCELL-ST vary between 250 and 500 nm, whereas the skin of CV is thicker, varying between 500 and 1000 nm. The maps of crystallinity index and degree of orientation of CV indicate a clearer distinction between the “skin” and core compared to Ioncell fibers. The overall crystallinity index and degree of orientation of IONCELL-ST and IONCELL-HT are much higher than those of CV. This is consistent with previous macroscopic measurements (Moriam, K. et al. 2021; Jiang G. et al. 2012).[16,17] The high crystallinity index and degree of orientation of Ioncell fibers are indicative of well-ordered structures, and can contribute to the superior mechanical properties. However, structural variations of microfibrils are not observed among different types of fibers. SEM shows that MFs of CV have a size of

~100 nm (Müller, M. et al. 2000; Schuster K. C. et al 2002). A qualitative analysis of the SAXS results in Figure S8 confirms that the microfibril sizes of IONCELL-HT, IONCELL-ST and CV are comparable. Thus, the difference in the mechanical properties of different types of fibers is most likely due to the structural variations of the elementary fibrils.

4.2 The meso-structural variations of elementary fibrils for different fibers.

The crystallinity, amorphous orientation and the orientation of voids are strongly correlated with the mechanical strength of regenerated fibers (Jiang G. et al 2012; Schurz J. & Lenz J. 1994; Sharma, A. et al. 2019; Sharma, A. et al 2021). While the longitudinal structural features have been well studied previously, the transverse structures of microfibrils and elementary fibers have not been fully elucidated. It had been found that different kinds of man-made cellulosic fibers spun from different solvent systems had a similar structural arrangement of elementary fibrils, which was represented by a lamella model having a period of ~6-8 nm (Lenz J. et al 1988). This provides an estimation of inter-fibrils spacing between elementary fibrils.

Through studying the variations of interference patterns at $q = 0.17$ Å^{-1} in the scanning measurements, we reveal the meso-structural difference of elementary fibrils of different fiber types. The fitting results using Monte Carlo simulations, shown in Figure 3a, indicate that the elementary fibril of IONCELL-HT have elongated ribbon-shapes with a cross-section of about 6x2 nm. The elementary fibrils have a preferred orientation in the elongated direction of their cross sections. This is consistent with the morphology of cellulose II nanowhiskers (average widths 4.2±1.5 nm (AFM), TEM 6.3 nm±1.5 nm) and TEMPO-oxidized cellulose II nanoelements (TEM 4-12 nm width) (Hirota, M. et al 2012; Sèbe, G. et al 2012). Figure S11 shows that increasing the volume fraction of elementary fibrils within microfibrils can shift the peak to slightly higher q, and that increasing the width of the orientation distribution of the elementary fibrils results in a modest flattening of the interference patterns. Nonetheless, as can be seen in Figure 3b, an increase in heterogeneity of the elementary fibrils' morphology can flatten the interference patterns. Although the fitting results show that elementary fibrils of IONCELL-ST exhibit a greater size variation than those of IONCELL-HT, they both maintain a preferential orientation. Figure 3c shows that the SAXS curve of CV contains no significant interference patterns, in stark contrast to the strong interference seen in scattering from IONCELL-HT and IONCELL-ST. The fitting results indicate that the structure of the elementary fibrils of CV has a lower structural order than those of IONCELL fibers. Both the size and shape of the elementary fibrils of CV vary widely. The orientation is also more random as well. Thus, the well-oriented elementary fibrils of Ioncell fibers generate narrow and elongated voids within MFs, while the voids within microfibrils of CV are larger than those of Ioncell fibers.

4.3 The Molecular structural variation of elementary fibrils for different fibers.

The variations of the equatorial WAXS profiles of different regenerated cellulose fibers indicate that the spinning process has an impact on the nanostructures of the elementary fibrils. Considering the size limits of the elementary fibrils, we created nine representative explicit models for fitting the equatorial WAXS profiles. The 020 reflection of CV shows higher intensity than the 110 reflection. This is consistent with the theoretical calculation of the cylindrically averaged intensity profile. The intensity profile containing a stronger 020 has been found for thinly cut CV (Gindl-Altmutter, W., et al. 2014). The intensity profile determined by a spherical mean instead of a cylindrical mean, therefore, will observe a stronger 110 for the whole fiber due to the contribution of the 021 reflection (Gindl-Altmutter, W., et al. 2014). The uniform alignment of the microfibrils for a thin section compensated for the distortion of the spherical averaging, resulting in a stronger 020 reflection (Gindl-Altmutter, W., et al. 2014). Of particular interest is the observation that the equatorial WAXS profiles of IONCELL-HT and IONCELL-ST show stronger 110 reflection than 020. This indicates that the cellulose sheets within elementary fibrils have a preferential stacking direction along 1-10 direction. The preferential stacking direction along 1-10 will increase the hydrophobic surface of elementary fibrils. These structural differences could be due to the different spinning process for Viscose and Ioncell fiber regeneration. The Viscose process is regenerated in an acidic bath in which the xanthate is saponified and converted into cellulose again, which cause the coagulation and regeneration happening simultaneously. The cellulose is crystallized in aqueous environment, which will minimize the hydrophobic surface of cellulose fibrils. The Ioncell process, in contrast, is based on a dry-jet-wet spinning process. The fibers are spun through an air gap aiming at reducing the moisture during crystallization (Azimi, B. et al., 2022). This way enables the formation of elementary fibrils of Ioncell fibers having a larger hydrophobic surface. Dry-jet-wet spinning is also characterized by a high stretch ratio (Azimi, B. et al., 2022). For the Ioncell process, the preordered spinning solution in which the cellulose molecules were oriented lengthwise in the spinning direction could lead to a higher crystallinity but less clustering of elementary fibrils.[18] These pre-oriented cellulose molecules could initially form cellulose sheets, and then further assemble as elementary fibrils. This crystallization process could be promoted by the shearing force. Thus, the nascent elementary fibrils might endure high shear forces during dry-jet-wet spinning of Ioncell fibers. However, it is unclear to what extent the shear force leads to higher crystallinity and more uniform dimensions of the elementary fibrils.

4.4 The homogeneity of morphologies of elementary fibrils is essential for high tenacity of RCFs.

Higher porosity will lead to a lower volume density of fibrils, and furthermore, pores represent defects that reduce the mechanical properties. Thus, to achieve high tenacity, regenerated fibers need to have lower porosity. SEM and SAXS show that CV contains cavities of a few hundred nm in size, whereas IONCELL fibers have a uniform and condensed inner structure (Schuster, K.C. et al 2003). Thus, Ioncell fibers exhibit much higher CI and DPO but lower porosity than CV which could explain the overall high tenacity.

There are no obvious cavities observed within both IONCELL fibers by SEM (Abu-Rous, M., et al., 2006). However, IONCELL-HT exhibits extreme tenacity. The molecular weight distribution of the cellulose has an influence on the rheology of the IONCELL spinning solutions as well as on the spinning behavior and the properties of the resulting fibers. (Michud A. et al. 2015, Ma Y. et al. 2023) Here we focused on structural perspective. The high structural homogeneity of the elementary fibrils of IONCELL-HT allows a better distribution of tensile stress. The elementary fibrils of IONCELL-ST are more polydisperse in cross section than IONCELL-HT. The heterogeneity of elementary fibrils leads to unequal stress concentration within microfibrils. The larger elementary fibrils within IONCELL-ST could only bear additional stress and break easier as the stress increases. Consequently, fracturing elementary fibrils could increase the stress on residual elementary fibrils and reduce their tenacity. This consequential reaction means that the inhomogeneity of elementary fibrils within MFs could limit the toughness of RCFs

Table 1. The mechanical properties of IONCELL-HT, IONCELL-ST and CV fibers.

Sample name	**Linear density (dtex)**	**Tenacity (cN/dtex)**	**Elongation (%)**	**Length of the fiber (mm)**	**DR**	**Pulp**	**Solvent**
High tenacity Ioncell (HT)	0.97	59.27	14.3	4	10	Buckeye	[DBNH][OAc]

Standard Ioncell (ST)	1.25	49.49	11.35	8	11	Enocell	[DBNH][OAc]
Viscose fiber (CV)	1.32	19.54	18.62	4			

4.5 The effect of structural variation on wet mechanical properties.

The SAXS interference peak was more pronounced and shift the q of maximum to lower value under wet condition (Schruz, J., & Lenz, J. 1994). These variations of SAXS result indicate that the IONCELL fibers preserve the monodispersity of elementary fibrils and enlarge the inter-fibrillar distance. The uniformity of elementary fibrils of IONCELL allows the uniform penetration of moisture (Abu-Rous, M., et al., 2006). In addition, WAXS of IONCELL fibers indicates elementary fibrils having a larger hydrophobic surface, which prevents interaction with water molecules and promotes moisture transfer. This conform to the changes of moisture contents of fibers affected by the relative humidity. (Figure S18) The good “wet” strength properties of IONCELL fibers suggest that increasing hydrophobicity or the homogeneity of elementary fibrils or both could result in their superior mechanical properties. To confirm the correlation between structure and “wet” mechanical properties, a comprehensive characterization of structural information of different fibers under different moisture conditions is necessary in future.

5. CONCLUSIONS

This study provides a comprehensive characterization of the structure of regenerated cellulose fibers as a basis for understanding the different mechanical properties of fibers fabricated through different processes. A schematic fiber structure (Figure 6a) reveals that all types have a "skin-core" morphology, with the thickness of the skin being 250-1000 nm. Regular viscose fiber has a slightly thicker “skin” than IONCELL-HT and IONCELL-ST. The main structural difference between the “skin” and “core” for Ioncell fibers is that the “skin” has much larger porosity than the “core”. The microfibril diameters were universally around 100 nm. The structure of the elementary fibrils within the microfibrils varies according to the different spinning processes. In Ioncell dry-jet wet-spinning, they are ribbon-like with a size of 6x2 nm. The high crystallinity index and orientation parameter of Ioncell fibers indicates that cellulose forms homogeneous elementary fibrils instead of coagulating as individual large crystal (Figure 6b). On the other hand, the elementary fibrils of CV have a broader size, shape and orientation distribution (Figure 4b). The equatorial WAXS profiles of IONCELL-HT and IONCELL-ST show stronger 110 than 020 reflection, contrary to CV. This indicates that the cellulose sheets of elementary fibrils of Ioncell fiber are predominantly stacked along the 1-10 direction(Figure 6c). In sum, the great uniformity and the increase of hydrophobicity of the elementary fibrils of IONCELL fibers on the meso and molecular level are crucial for the high strength of regenerated fibers. The homogeneity of elementary fibrils and the additional hydrophobicity due to the direction of crystal growth during coagulation of IONCELL could allow uniform moisture penetration, which in turn could enable good wet mechanical properties by avoiding stress concentration.

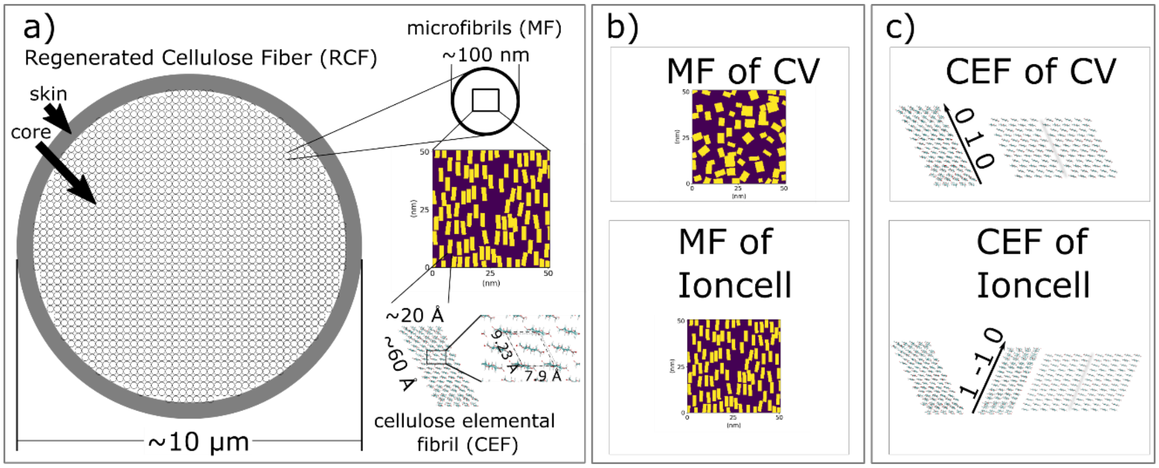

Figure 6. The schematic of hierarchical structure of RCF and the structural differences of elementary fibrils (CEFs) on meso and molecular scale between Ioncell and Viscose process. a) Hierarchical structure of RCFs. Fiber has “skin-core” structure. The size of skin is around 0.2-1 micron. The core region is made up of MFs having diameter of ~100 nm. Within MFs, CEFs of IONCELL-HT form as elongated ribbon having a length of ~ 6nm and a width of ~2nm. The lattices of cellulose crystal have decreased in (1 0 0) direction and increased in (0 1 0) direction. b) Meso-structural variation of CEFs within MFs for spinning process. The CEFs of CV are highly random in size and shape of orientation. In contrast, the CEFs of IONCELL-HT exhibit higher homogeneity. c) Molecular structural difference of CEFs for different RCFs. In the IONCELL process cellulose sheets within CEFs stack preferably along (1 -1 0) direction, while CEFs of CV do not show a preferred stacking direction along (1 -1 0).

AUTHOR INFORMATION

Corresponding Author

*Manfred Burghammer
burgham@esrf.fr

* Yoshiharu
yoshiharu.nishiyama@cermav.cnrs.fr

Author Contributions

JL and YN conceived the project. MH and HS prepared the samples, JL and MB conducted the scanning microdiffraction experiments, MS conducted and analyzed the HRSAXS experiment, OY and YN conducted and analyzed ssNMR and FTIR measurements, JL and MB analyzed the scanning microdiffraction data, JL wrote the manuscript, all had discussed the results and edited the manuscript.

Funding Sources

This is an inhouse research project supported by ESRF. This has been supported by Business Finland through the project "From cellulose to new Finnish manmade cellulose fibers and sustainably colored textiles" (43619/31/2020).

Notes

The authors declare no competing financial interest.

ACKNOWLEDGMENT

We thank Dr. Makowski for the constructive discussions and critical reading of the manuscript. This project is supported by ESRF inhouse research projects at ID02 and ID13. Michael Hummel gratefully acknowledges support from Business Finland through the project "From cellulose to new Finnish manmade cellulose fibers and sustainably colored textiles" (43619/31/2020).

REFERENCES

Abu-Rous, M., Ingolic, E. and Schuster, K.C., 2006. Visualisation of the nano-structure of Tencel®(Lyocell) and other cellulosics as an approach to explaining functional and wellness properties in textiles. Lenzinger Berichte, 85, pp.31-37.

Asaadi, S., Hummel, M., Ahvenainen, P., Gubitosi, M., Olsson, U. and Sixta, H., 2018. Structural analysis of Ioncell-F fibres from birch wood. Carbohydrate polymers, 181, pp.893-901.

Azimi, B., Maleki, H., Gigante, V., Bagherzadeh, R., Mezzetta, A., Milazzo, M., Guazzelli, L., Cinelli, P., Lazzeri, A. and Danti, S., 2022. Cellulose-based fiber spinning processes using ionic liquids. Cellulose, pp.1-51.

Elsayed, S., Hummel, M., Sawada, D. *et al.* Superbase-based protic ionic liquids for cellulose filament spinning. *Cellulose* **28**, 533–547 (2021). https://doi.org/10.1007/s10570-020-03505-y

Gindl-Altmutter, W., Eichhorn, S.J., Burghammer, M. and Keckes, J., 2014. Radial crystalline texture in a lyocell fibre revealed by synchrotron nanofocus wide-angle X-ray scattering. Cellulose, 21(1), pp.845-851.

Guinier, A., 1994. X-ray diffraction in crystals, imperfect crystals, and amorphous bodies. Courier Corporation.

Hammouda, B., 2012. Probing Nanoscale Structures - The SANS Toolbox. The SANS Toolbox.

Hermanutz, F., Vocht, M.P., Panzier, N. and Buchmeiser, M.R., 2019. Processing of cellulose using ionic liquids. Macromolecular Materials and Engineering, 304(2), p.1800450.

Hirota, M., Tamura, N., Saito, T. and Isogai, A., 2012. Cellulose II nanoelements prepared from fully mercerized, partially mercerized and regenerated celluloses by 4-acetamido-TEMPO/NaClO/NaClO2 oxidation. Cellulose, 19(2), pp.435-442.

Jiang, G., Huang, W., Li, L., Wang, X., Pang, F., Zhang, Y. and Wang, H., 2012. Structure and properties of regenerated cellulose fibers from different technology processes. Carbohydrate Polymers, 87(3).

Lenz, J., Schurz, J. and Wrentschur, E., 1992. Comparative characterization of solvent spun cellulose and high wet modulus viscose fibres by their long periods. Acta polymerica, 43(6), pp.307-312.

Lenz, J., Schurz, J. and Wrentschur, E., 1988. The fibrillar structure of cellulosic man- made fibers spun from different solvent systems. *Journal of applied polymer science*, *35*(8), pp.1987-2000.

Liu, J., Bengtsson, J., Yu, S., Burghammer, M. and Jedvert, K., Variation in the hierarchical structure of lignin-blended cellulose precursor fibers. 2022 *International journal of biological macromolecules*, pp.S0141-8130.

Ma Y., You X., Nieminen K., Sawada D., Sixta H., 2023. Influence of DP and MMD of the pulps used in the Ioncell® process on processability and fiber properties. RSC Sustainability, DOI: 10.1039/D3SU00013

Michud A., Hummel M., Sixta H., 2015. Influence of molar mass distribution on the final properties of fibers regenerated from cellulose dissolved in ionic liquid by dry-jet wet spinning. Polymer, 75, pp1-9

Moriam, K., Sawada, D., Nieminen, K., Hummel, M., Ma, Y., Rissanen, M. and Sixta, H., 2021. Towards regenerated cellulose fibers with high toughness. Cellulose, 28(15), pp.9547-9566.

Moss, C.E., Butler, M.F., Müller, M. and Cameron, R.E., 2002. Microfocus small‐ angle X‐ ray scattering investigation of the skin–core microstructure of lyocell cellulose fibers. Journal of applied polymer science, 83(13), pp.2799-2816.

Müller, M., Riekel, C., Vuong, R. and Chanzy, H., 2000. Skin/core micro-structure in viscose rayon fibres analysed by X-ray microbeam and electron diffraction mapping. Polymer, 41(7), pp.2627-2632.

Müller, M., Czihak, C., Vogl, G., Fratzl, P., Schober, H. and Riekel, C., 1998. Direct observation of microfibril arrangement in a single native cellulose fiber by microbeam small-angle X-ray scattering. Macromolecules, 31(12), pp.3953-3957.

Nishiyama, Y., Asaadi, S., Ahvenainen, P. *et al.* Water-induced crystallization and nano-scale spinodal decomposition of cellulose in NMMO and ionic liquid dope. Cellulose **26**, 281–289 (2019). https://doi.org/10.1007/s10570-018-2148-x

T. Narayanan, M. Sztucki, T. Zinn, J. Kieffer, A. Homs-Puron, J. Gorini, P. Van Vaerenbergh and P. Boesecke, 2022. Performance of the time-resolved ultra-small-angle X-ray scattering beamline with the Extremely Brilliant Source. Journal of applied crystallography, 55, pp. 98-1111.

Ogawa, Y. and Putaux, J.L., 2019. Transmission electron microscopy of cellulose. Part 2: technical and practical aspects. Cellulose, 26(1), pp.17-34.

Sèbe, G., Ham-Pichavant, F., Ibarboure, E., Koffi, A.L.C. and Tingaut, P., 2012. Supramolecular structure characterization of cellulose II nanowhiskers produced by acid hydrolysis of cellulose I substrates. Biomacromolecules, 13(2), pp.570-578.

Schuster, K.C., Aldred, P., Villa, M., Baron, M., Loidl, R., Biganska, O., Patlazhan, S., Navard, P., Rüf, H. and Jericha, E., 2003. Characterising the emerging lyocell fibres structures by ultra small angle neutron scattering (USANS). Lenzinger Berichte, 82, pp.107-117.

Schurz, J. & Lenz, J., 1994. Investigation of the structure of regenerated cellulose fibers. Macromolecules Symposium, Volume 83, pp. 273-289.

Sharma, A., Sen, D., Thakre, S. and Kumaraswamy, G., 2019. Characterizing microvoids in regenerated cellulose fibers obtained from viscose and lyocell processes. Macromolecules, 52(11), pp.3987-3994.

Sharma, A., Wankhede, P., Samant, R., Nagarkar, S., Thakre, S. and Kumaraswamy, G., 2021. Process-induced microstructure in viscose and lyocell regenerated cellulose fibers revealed by SAXS and SEM of acid-etched samples. ACS Applied Polymer Materials, 3(5), pp.2598-2607.

Williams, T. and Kelley, C. (2011). Gnuplot 4.5: an interactive plotting program. URL http://gnuplot.info.